Arabian Journal of Chemistry (2021) **14**, 102939

King Saud University

Arabian Journal of Chemistry

www.ksu.edu.sa
www.sciencedirect.com

ORIGINAL ARTICLE

Lumped kinetic model for degradation of chitosan by hydrodynamic cavitation

Tianyu Wang, Pengfei Wang, Kunming Zhang, Feng Yang, Yongchun Huang *, Chengdu Huang

Guangxi Key Laboratory of Green Processing of Sugar Resources (Guangxi University of Science and Technology), Liuzhou 545006, Guangxi, PR China
School of Biological and Chemical Engineering, Guangxi University of Science and Technology, Liuzhou 545006, Guangxi, PR China

Received 6 September 2020; accepted 9 December 2020
Available online 19 December 2020

KEYWORDS

Hydrodynamic cavitation;
Chitosan;
Degradation;
Lumped;
Kinetic;
Reaction network

Abstract The lumped kinetic model for the degradation reactions of chitosan by hydrodynamic cavitation was investigated in this study. The molecular weight distributions and mass concentrations were determined by gel permeation chromatograph (GPC). The degradation products were divided into several lumps according to their molecular weights. The appropriate number of lumps for the kinetic study was determined by comparing the residual sum of squares (RSS) values among different models. The RSS of six-lumped model (5.36×10^{-3}) was relatively small and the estimation of parameters was simpler than other models. In this paper, six-lumped kinetic model was adopted and the corresponding reaction network was established. The kinetic parameters were estimated with the Levenberg-Marquardt, and the results showed that the degradation reaction of chitosan was mainly dominated by the formation of degradation products with similar molecular weights. The maximum value of kinetic parameters on the diagonal of the reaction network (1.63×10^{-1}) was much larger than that of non-diagonal kinetic parameters (3.78×10^{-2}). According to the results calculated and measured under different conditions, this model could accurately predict the concentration distributions of lumps in the reaction network, and most of the average absolute deviation were smaller than 9.3%.

1. Introduction

Chitosan, β-(1–4)-2-amino-2-deoxy-b-D-glucan, is a natural polymer derived from the deacetylation of chitin isolated from crustacean shells (Negm et al., 2020). Chitosan and its derivatives have interesting properties such as nontoxicity, biocompatibility, antimicrobial activity (Zou et al., 2016), controllable biodegradability and nonantigenicity, making chitosan an attractive biopolymer for applications in many fields

* Corresponding author.
E-mail address: huangyc@yeah.net (Y. Huang).
Peer review under responsibility of King Saud University.

Production and hosting by Elsevier

https://doi.org/10.1016/j.arabjc.2020.102939

such as biotechnology (Kumar, 2000), pharmaceuticals (Czech et al., 2020), wastewater treatment (Iovino et al., 2016), cosmetics, agriculture, food science, and textiles (Rinaudo, 2006). The characteristics of chitosan are dependent on its molecular weight. For example, Song et al. (2020) found that the zero-valent selenium nanoparticles stabilized by chitooligosaccharide showed marked antitumor activity. Mei et al. (2015) evaluated the anti-dermatophytic activity in vitro and in vivo of a well-characterized chitooligosaccharide sample obtained by hydrolysis with a recombinant chitosanase. The sample exhibited significant clinical efficacy against der-matophytic infection caused by T.rubrum. Zaharoff et al. (2007) reported that a chitosan solution improved the humoral and cell-mediated immunity to a protein antigen in the absence of additional adjuvants.

Organics can be degraded by several methods, including acid hydrolysis (Lee et al., 1999), oxidative degradation (Tian et al., 2004), enzymatic degradation (Kim and Rajapakse, 2005), photodegradation (Liu et al., 2019) and degradation by hydrodynamic cavitation. During the process of hydrodynamic cavitation, vapor bubbles are formed in aqueous solutions because of the variation of pressure (Chuah et al, 2016). These bubbles collapse violently in high-energy environment after growing (Chuah et al, 2015). In aqueous solutions, radicals, especially hydroxyl radicals, are produced. It was reported that hydrodynamic cavitation could be used for the degradation of organic compounds (Capocelli et al., 2013). Compared with other degradation methods, hydrodynamic cavitation possesses many advantages such as convenient operations, high efficiency, more uniform cavitation fields than ultrasonic cavitation (Muley et al., 2019), energy efficiency, shorter reaction time, economic point of views as well as the potential for future implementation and development in industries (Chuah et al., 2017). In the previous work, chitosan degradation by hydrodynamic cavitation with an orifice plate, turbine, Venturi tube and organ-pipe were performed, and the impact of concentration, deacetylation degree, temperature, pH, pressure, time, orifice plate structure, Venturi and organ-pipe structures on the performance of degradation were discussed. The results indicated that chitosan can be effectively degraded by hydrodynamic cavitation. Huang et al. (2013) found that the degradation efficiency increased with increasing temperature, treatment time and pressure, and decreased with increasing solution concentration. Wu et al. (2014) reported that orifice plates with larger numbers of holes and smaller hole diameters could increase the intensity of cavitation and improve the chitosan degradation performance. Huang et al. (2015) found that the inlet and outlet angles of Venturi tube obviously affected the degradation performance of chitosan and the synergistic degradation with impinging stream and jet cavitation was significantly better than that of single jet cavitation. Yan et al. (2020b) performed the chitosan degradation experiments by using an organ-pipe. The results showed that the degradation efficiency was significantly improved by self-resonating cavitation.

The kinetics is one of the important research fields of chitosan degradation. However, most work focused on the development of products and optimization of experimental conditions. There are few studies on the mechanism of chitosan degradation. Degradation reactions of chitosan are a complicated system, which contains many components and numerous reactions (Huang et al., 2013). For example, a component could act as both product and reactant in different reactions. Parallel reactions exist with consecutive reactions simultaneously. The kinetic behaviors of components was unable to quantitatively describe (Shi et al., 2005). It is difficult to determine the molecular weight distribution of degraded chitosan. Using conventional experimental method to study the kinetics of these complex reaction systems is hard.

In this work, a novel six-lumped kinetic model was established to study the degradation reactions of chitosan by hydrodynamic cavitation based on the characteristics of hydrodynamic cavitation and research strategies in petrochemical industry (Zhang et al., 2017). First, the reaction system was divided into several lumps based on the different physiological activities of chitosan with different molecular weights (John et al., 2019). Then, the lumps with similar kinetic properties are combined to establish a six-lumped kinetic model. Then, model fitting and parameters estimation using a nonlinear least square method were achieved by the Matlab software. This model is of great significance to the mechanism research of chitosan degradation by hydrodynamic cavitation, optimization of degradation conditions and determination of product distributions. This method can be also applied to the reaction kinetics investigations of similar complicated systems involving polysaccharides, lipids and nucleic acids.

2. Materials and methods

2.1. Materials

Chitosan (deacetylation degree > 90%) was obtained from Kabo Industrial Co., Ltd. (Shanghai, China). Acetic acid (CH_3COOH) and sodium acetate (CH_3COONa) were purchased from Chengdu Kelong Chemical Reagent Factory. Glucan was purchased from Waters, USA. Deionized water was provided with a conductivity of 4 μs/cm.

2.2. Instruments

The experimental analysis was measured with a Waters gel permeation chromatograph equipped with an Ultrahydrogel column (Milford, Massachusetts, USA), 2414 refractive index detector and 1515 pump. The hydrodynamic cavitation field was generated in a home-made reactor equipped with a magnetic pump (1/2DW-750, rated voltage/power: 200 V/750 W, Zhejiang Aolong Technology Development Co., Ltd. China) and pressure guages (0.6 Mpa, Hangzhou Guanshan Instrument Co., Ltd. China).

2.3. Methods

Fig. 1 shows the schematic of the experimental setup for hydrodynamic cavitation. It consists of a closed-loop system. The chitosan solution was drawn from a tank, and transferred into the impinging reactor and jet cavitation reactor with two magnetic pumps through the values V_1, V_2 and V_3. Then, the solution was discharged into the tank. In the reactors, jet cavitation was generated by using a Venturi tube, which is illustrated in Fig. 2.

The optimized chitosan degradation conditions adopted in this experiment were found by Huang et al. (2015). 3 L of a 3 g/L chitosan solution (pH = 4.4; contained 0.2 mol/L CH_3-

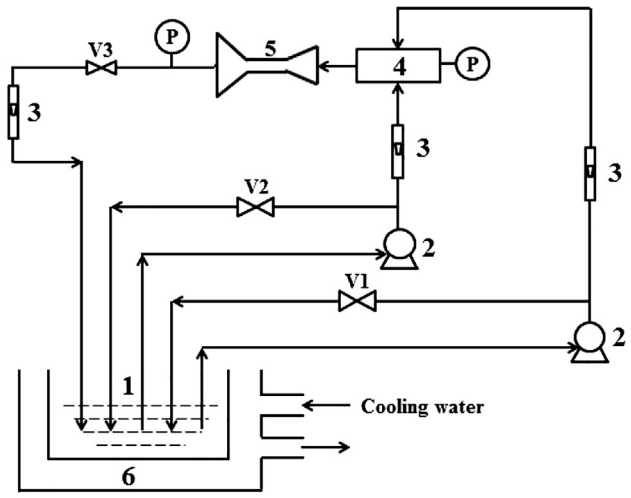

Fig. 1 Schematic presentation of the experimental setup for hydrodynamic cavitation. 1-holding tank; 2-magnetic pump; 3-rotameter; 4-impinging reactor; 5-jet cavitation reactor; 6-cooling water; V1, V2, V3-valve.

COOH and 0.1 mol/L CH_3COONa) was poured into the tank. The magnetic pumps were initiated. The reactions were performed for 120 min, and samples were withdrawn every 5 min, under the conditions of pH of 4.4, and inlet pressure of 0.4 Mpa (adjusted by the valves V_1 and V_2). The experiments were performed at different temperatures (30 °C, 35 °C, 40 °C, 45 °C, 50 °C and 60 °C). The inlet and outlet angles of the Venturi tube in the hydrodynamic cavitation device were adjusted to be 60 °and 76°, and the length and diameter of the throat were measured to be 10 and 4 mm.

2.4. Characterization

The molecular weights and its distributions of the products were measured by gel permeation chromatography (GPC) with a mobile phase comprising 0.2 mol/L CH_3COOH and 0.1 mol/L CH_3COONa and a flow rate of 0.6 mL/min (Moore, 1964). 25 μL sample was detected with the sensitivity of 32 under detector and column temperatures of 30 °C. The glucan standard was used to calibrate the molecular weights of chitosan samples (Ren et al., 2006).

After the degradation by hydrodynamic cavitation, the concentrations of degradation products were quantified by GPC with a five-point calibration curve (0.9, 1.2, 1.5, 1.8, and 2.1 mg/mL) (Lee and Chang, 1996).

3. Results and discussion

3.1. Models establishment

Before the establishment of models, some hypotheses necessary are presented as follows:

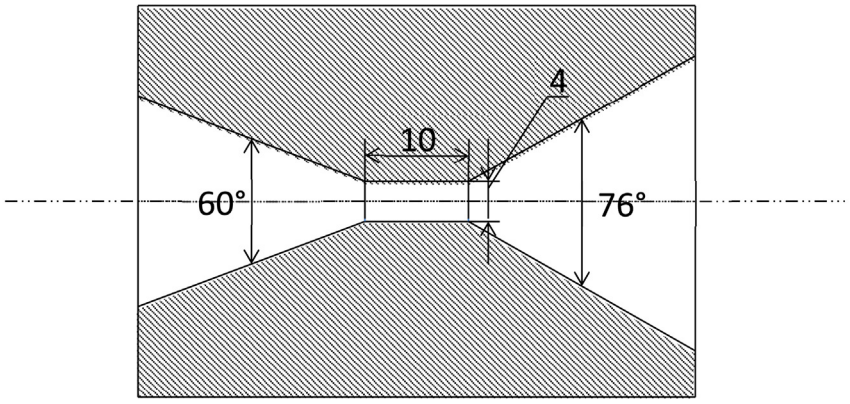

(a)

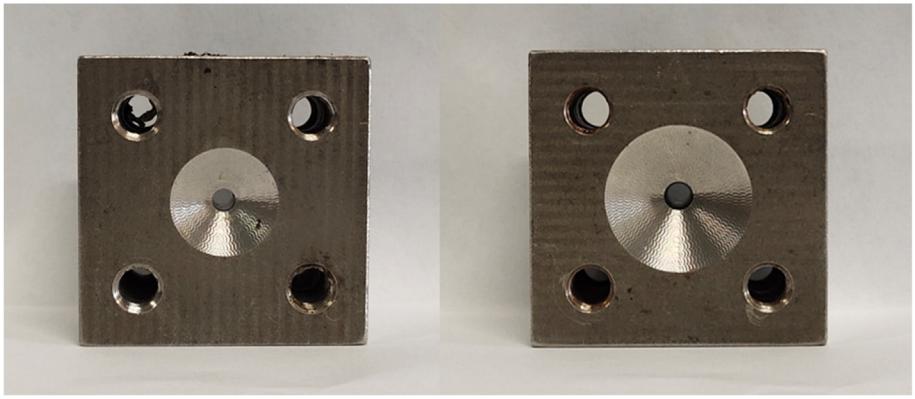

(b)

Fig. 2 Structure of Venturi tube (a) Photograph of Venturi setup (b).

A. The degradation of chitosan follows the first-order reaction kinetics.
B. Chitosan degradation products with similar molecular weights have similar kinetic characteristics in the reaction system. The lumps were divided according to the molecular weights of products. The components in a lump do not interact with each other.
C. The lump with high molecular weights can be degraded into another lump with low molecular weights. The lowest lump will not be degraded anymore. The reaction rates of different lumps are different. Moreover, no reverse reactions take place.
D. The reactions take place in a homogeneous solution, so the influence of molecular diffusion will be ignored.
E. The hydrodynamic cavitation degradation of chitosan agrees with the rules of random degradation.

The lumps were divided by their molecular weights which are one of the most important parameters of chitosan, because the kinetic properties will be affected by the molecular weights. For example, oligochitosan has certain inhibitory effects on fungi and microorganisms when the average molecular weights were in the range of 5 kDa ~ 10 kDa (Kyoon No et al., 2002). The oligochitosan with molecular weights of 1.5 kDa and 3 kDa showed excellent water solubility (Mourya et al., 2011), moisture absorption, moisture retention and other properties (Xia et al., 2011). The whole system should be subdivided according to the physiological activities before the appropriate lump number was determined.

The reaction system was divided into n lumps based on the hypotheses. The network established is shown in Fig. 3. In this reaction network, molecular weights decrease from A_1 to A_n. If the reaction of each step exists, the number of reactions (N_r) equals $n(n\text{-}1)/2$. Building on the hypotheses and the n-lumped reaction network, the differential equations representing the reactions of these lumps are shown as follow:

$$\frac{dc_{A_1}}{dt} = -(k_{11} + k_{12} + k_{13} + \ldots + k_{1(n-1)})c_{A_1} \quad (1)$$

$$\frac{dc_{A_2}}{dt} = k_{11}c_{A_1} - (k_{21} + k_{22} + \ldots + k_{2(n-2)})c_{A_2} \quad (2)$$

$$\frac{dc_{A_3}}{dt} = k_{12}c_{A_1} + k_{21}c_{A_2} - (k_{31} + \ldots + k_{3(n-3)})c_{A_3} \quad (3)$$

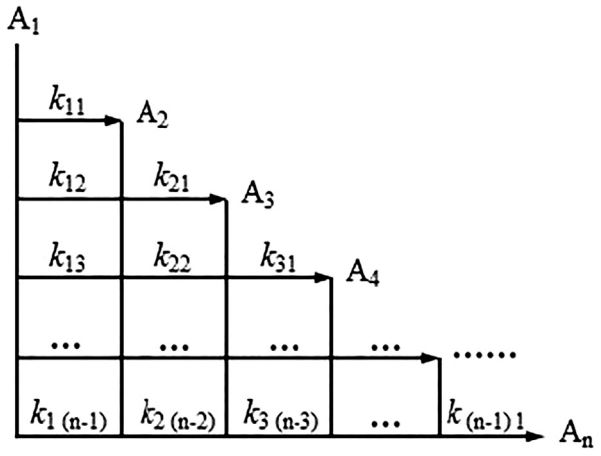

Fig. 3 Reaction network for n lumps.

$$\frac{dc_{A_n}}{dt} = k_{1(n-1)}c_{A_1} + k_{2(n-2)}c_{A_2} + \ldots + k_{(n-1)1}c_{A_{(n-1)}} \quad (4)$$

As mentioned before, there are $n(n\text{-}1)/2$ reactions. Since each reaction contains a reaction rate constant k_{ij}, a total of $n(n\text{-}1)/2$ parameters are unknown. The equations are mass balances.

3.2. Trade-off of the number of lumps

The whole degradation system was divided into 12 lumps according to the analysis results in section **3.1**. The molecular weights of A_1 to A_{12} are above 1000 kDa, 800 kDa ~ 1000 kDa, 500 kDa ~ 800 kDa, 300 kDa ~ 500 kDa, 200 kDa ~ 300 kDa, 100 kDa ~ 200 kDa, 80 kDa ~ 100 kDa, 50 kDa ~ 80 kDa, 30 kDa ~ 50 kDa, 10 kDa ~ 30 kDa, 5 kDa ~ 10 kDa, and below 5 kDa. The concentrations of degradation products at different times are shown in Table 1. The changing trends of mass concentrations over time are shown in Fig. 4**(a)**. The concentrations of lumps A_3, A_4 and A_5 increased first, and then decreased slowly, showing similar kinetic behaviors. Same phenomenons were observed in the profiles of lumps A_9 and A_{10}, A_{11} and A_{12}. The lumped kinetics research method combines components into certain groups, of which the kinetic behaviors are similar. The number of variables and parameters can be reduced and a complicated system can be simplified (Shi et al., 2005). Based on these fundamental principles of lumped kinetics and experimental results, eight-lumped model was obtained by combing the above lumps with similar kinetic behaviors.

According to the above-mentioned strategy, the eight-lumped model can be further merged into seven-lumped, six-lumped, five-lumped and four-lumped models. The fitting results and corresponding RSS values of these models are shown in Fig. 4**(b)~(f)** and Table 2. Among these models, the eight-lumped and six-lumped models, with the RSS values of 5.18×10^{-3} and 5.36×10^{-3}, exhibited better performances. The number of unknown kinetic parameters k_{ij} in the six-lumped model (15) was much smaller than those in the seven-lumped and eight-lumped models. For the four-lumped and five-lumped models, the RSS values were large, and the molecular weight ranges of products in all the lumps were too large, which may decrease the accuracy of parameters estimated. In the sections below, the six-lumped kinetic model was taken into account.

3.3. Six-lumped kinetic model and parameters estimation

3.3.1. Six-lumped kinetic model

The six-lumped kinetic model was established according to the analysis results in sections **3.1** and **3.2**. The ordinary differential equations are given as follows:

$$\frac{dc_{A_1}}{dt} = -(k_{11} + k_{12} + k_{13} + k_{14} + k_{15})c_{A_1} \quad (5)$$

$$\frac{dc_{A_2}}{dt} = k_{11}c_{A_1} - (k_{21} + k_{22} + k_{23} + k_{24})c_{A_2} \quad (6)$$

$$\frac{dc_{A_3}}{dt} = k_{12}c_{A_1} + k_{21}c_{A_2} - (k_{31} + k_{32} + k_{33})c_{A_3} \quad (7)$$

Table 1 Chromatographic quantitative analysis results of different time degradation products.

t(min)	0	5	10	15	20	25	30	35	40
Mw > 1000 kDa	0.5909	0.4773	0.3969	0.3357	0.2690	0.2186	0.1627	0.1286	0.0972
Mw800 ~ 1000 kDa	0.0694	0.0721	0.0718	0.0687	0.0638	0.0590	0.0521	0.0465	0.0393
Mw500 ~ 800 kDa	0.1393	0.1545	0.1612	0.1593	0.1537	0.1481	0.1388	0.1292	0.1143
Mw300 ~ 500 kDa	0.1339	0.1592	0.1759	0.1808	0.1834	0.1857	0.1874	0.1830	0.1706
Mw200 ~ 300 kDa	0.0890	0.1102	0.1271	0.1350	0.1426	0.1507	0.1617	0.1644	0.1598
Mw100 ~ 200 kDa	0.1111	0.1396	0.1677	0.1825	0.1991	0.2189	0.2498	0.2642	0.2666
Mw80 ~ 100 kDa	0.0278	0.0347	0.0430	0.0473	0.0524	0.0589	0.0702	0.0765	0.0789
Mw50 ~ 80 kDa	0.0457	0.0560	0.0701	0.0772	0.0858	0.0970	0.1186	0.1310	0.1369
Mw30 ~ 50 kDa	0.0345	0.0404	0.0518	0.0555	0.0620	0.0697	0.0858	0.0980	0.1034
Mw10 ~ 30 kDa	0.0402	0.0396	0.0581	0.0477	0.0555	0.0627	0.0748	0.0888	0.0992
Mw5 ~ 10 kDa	0.0103	0.0079	0.0154	0.0064	0.0064	0.0101	0.0109	0.0145	0.0169
Mw < 5 kDa	0.0058	0.0024	0.0092	0.0008	0.0009	0.0031	0.0031	0.0066	0.0057
Total mass concentration(mg/mL)	1.2979	1.2939	1.3483	1.2970	1.2745	1.2824	1.3160	1.3314	1.2889
t(min)	45	50	60	70	80	90	100	110	120
Mw > 1000 kDa	0.0740	0.0627	0.0403	0.0224	0.0151	0.0085	0.0039	0.0026	0.0009
Mw800 ~ 1000 kDa	0.0334	0.0298	0.0233	0.0152	0.0112	0.0073	0.0043	0.0029	0.0016
Mw500 ~ 800 kDa	0.1015	0.0937	0.0762	0.0570	0.0452	0.0323	0.0224	0.0159	0.0107
Mw300 ~ 500 kDa	0.1596	0.1534	0.1759	0.1378	0.1139	0.0988	0.0793	0.0623	0.1706
Mw200 ~ 300 kDa	0.1554	0.1548	0.1499	0.1340	0.1242	0.1088	0.0940	0.0799	0.0701
Mw100 ~ 200 kDa	0.2700	0.2786	0.2930	0.2817	0.2792	0.2633	0.2543	0.2344	0.2243
Mw80 ~ 100 kDa	0.0823	0.0870	0.0970	0.0980	0.1018	0.1025	0.1045	0.1018	0.1026
Mw50 ~ 80 kDa	0.1446	0.1554	0.1794	0.1865	0.1993	0.2081	0.2203	0.2233	0.2328
Mw30 ~ 50 kDa	0.1102	0.1207	0.1446	0.1540	0.1706	0.1856	0.2038	0.2163	0.2328
Mw10 ~ 30 kDa	0.1066	0.1158	0.1419	0.1586	0.1780	0.2089	0.2272	0.2544	0.2791
Mw5 ~ 10 kDa	0.0188	0.0193	0.0224	0.0299	0.0325	0.0443	0.0445	0.0536	0.0573
Mw < 5 kDa	0.0063	0.0066	0.0093	0.0115	0.0132	0.0188	0.0207	0.0260	0.0266
Total mass concentration(mg/mL)	1.2626	1.2777	1.3161	1.2628	1.2692	1.2707	1.2619	1.2598	1.2775

$$\frac{dc_{A_4}}{dt} = k_{13}c_{A_1} + k_{22}c_{A_2} + k_{31}c_{A_3} - (k_{41} + k_{42})c_{A_4} \quad (8)$$

$$\frac{dc_{A_5}}{dt} = k_{14}c_{A_1} + k_{23}c_{A_2} + k_{32}c_{A_3} + k_{41}c_{A_4} - k_{51}c_{A_5} \quad (9)$$

$$\frac{dc_{A6}}{dt} = k_{15}c_{A_1} + k_{24}c_{A_2} + k_{33}c_{A_3} + k_{42}c_{A_4} + k_{51}c_{A_5} \quad (10)$$

These differential equations correlate the mass concentrations of the six lumps with degradation time, and 15 unknown reaction rate constants k_{ij} are to be determined. The Levenberg-Marquart method (Huang, 2004) was used to estimate these 15 kinetic parameters by using the Isqnonlin function in the MATLAB software (Beers, 2006). Since the number of unknown variables of three-lumped reaction network equals the number of equations, several kinetic parameters k_{ij} could be obtained through calculations (Zhao et al., 2011). These k_{ij} values were further used to solve four-lumped, five-lumped and six-lumped equations. The Rung-Kutta method was chosen to get the numerical solutions of those ordinary differential equations by using the function ode45 in Matlab, with the data regarding the mass concentrations of lumps at different reaction times and temperatures. For the minimization of errors, the nonlinear least square method with the Isqnonlin function was used in the fitting and estimation of the kinetic parameters in the reaction network.

3.3.2. Estimation of lumped kinetic parameters

The degradation reactions were performed at 30, 40, 50 and 60 °C, and the products concentrations at different times were determined, as shown in Table 3.

The estimation values of reaction rate parameters and the comparison of experimental and calculation values at different temperatures are shown in Table 4 and Fig. 5. It can be seen that the reaction rate constants in the degradation of different lumps into other lumps were rather different.

For example, the reaction rate constants in the degradation of A_1 and A_2 into A_3, A_4, A_5 and A_6 were different. Under the condition of same degradation time, the reaction rate constants k_{13}, k_{14}, and k_{15} are relatively small in the degradation of A_1 with a greater molecular weight, while those (k_{22}, k_{23}, and k_{24}) are relatively large in the degradation of A_2 with a smaller molecular weight. In addition, the reaction rate constants k_{11}, k_{21}, k_{31}, k_{41} and k_{51} are large in the whole degradation process. The results illustrated that the degradation of chitosan mainly occurred on the diagonal of the six-lumped reaction network, and the reactions followed the path: $A_1 \rightarrow A_2 \rightarrow A_3 \rightarrow A_4 \rightarrow A_5 \rightarrow A_6$. This result may be caused by the chemical and mechanical effects in the hydrodynamic cavitation process. These effects led to different fracture sites in chitosan chains. The chemical effect led to random cuts and mechanical effect led to central cuts. As for the central cut, the cleavage took place at the middle points of the chitosan chains, and degradation products with larger molecular weights were prone to form. In random cuts, each linkage of the chitosan molecular chain had the same cleavage probability. It can be seen that the lump A_1 was more likely to degrade into lump A_2 rather than lumps A_3, A_4, A_5, and A_6 (Yan et al., 2020a). At 60 °C, the values k_{12}, k_{13}, k_{14}, k_{15} were low. This is probably because after the temperature reached a certain value, the coefficient of viscosity and surface tension of the solution decreased, and the vapor pressure of the solution increased. The cavitation threshold decreased, and cavitation

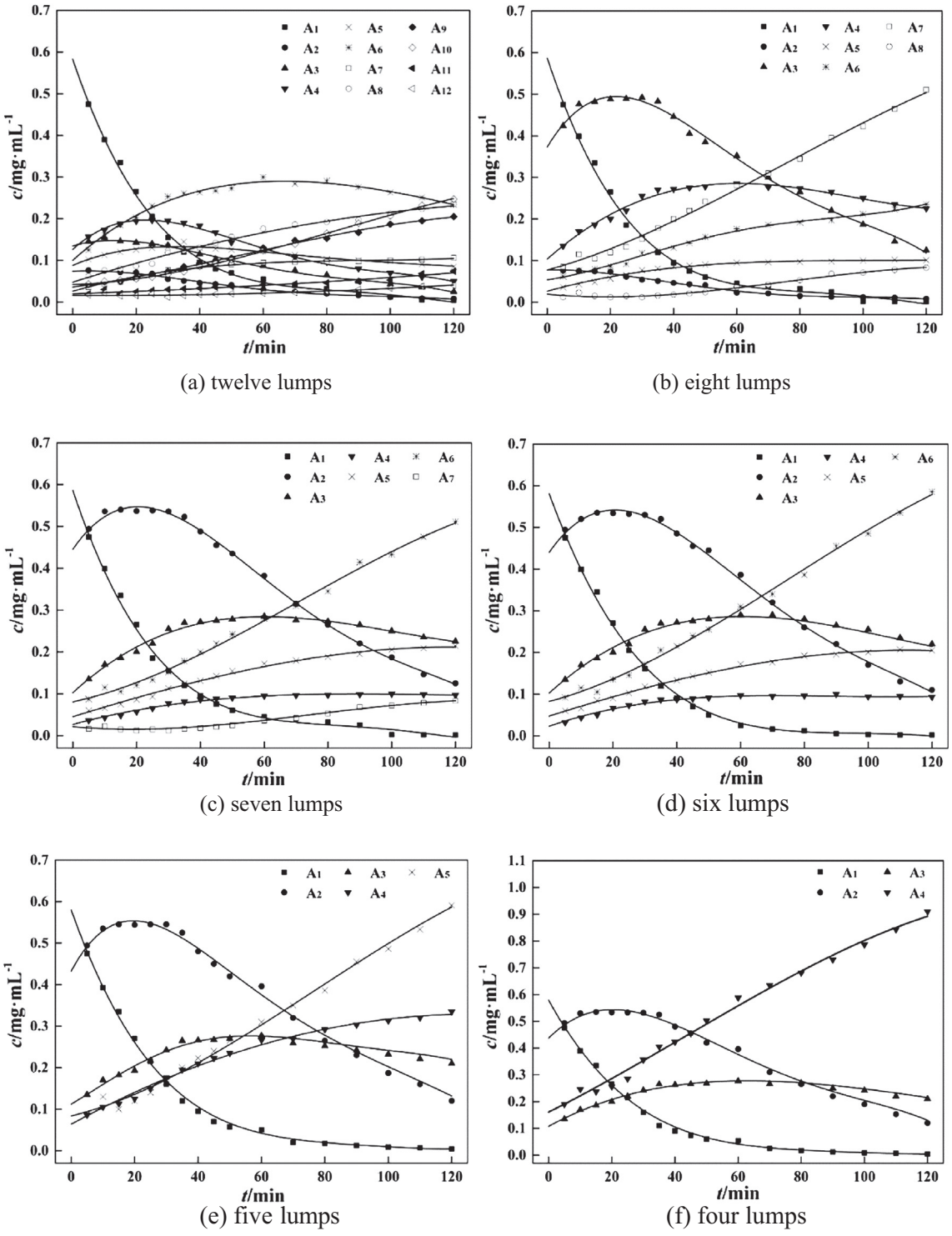

Fig. 4 Chitosan degradation curves for different lumps line-calculated value; dot-experimented value; t-degradation time; c-product concentration.

bubbles were easily produced. However, with the increase of temperature, the vapor pressure increased faster compared to the temperature of solution. The transient high temperature and high pressure generated by the collapse of cavitation bubbles decreased, reducing the intensity of cavitation, weakening the degradation rate. The similar situation was also observed by Huang et al. (2015) in the process of chitosan degradation. These results showed that the degradation reactions of chitosan led to the formation of lumps with similar molecular weights.

Analysis results in Table 4 indicate that six-lumped model was well fitted to the experimental values at different temper-

Table 2 Fitting results for different lumped kinetic models.

Lump	Eight lumps		Seven lumps		Six lumps		Five lumps		Four lumps	
	$M_W/\times10^4$	R^2	$M_W/\times10^4$	R^2	$M_W/\times10^4$	R^2	$M_W/\times10^4$	R^2	$M_W/\times10^4$	R^2
A_1 lump	> 100	0.9955	> 100	0.9951	> 100	0.9954	> 100	0.9954	> 100	0.9952
A_2 lump	80–100	0.9985	20–100	0.9948	20–100	0.9969	20–100	0.9967	20–100	0.9963
A_3 lump	20–80	0.9966	10–20	0.9842	10–20	0.9820	10–20	0.9804	10–20	0.9771
A_4 lump	10–20	0.9841	8–10	0.9859	8–10	0.9838	5–10	0.9945	< 10	0.9961
A_5 lump	8–10	0.9832	5–8	0.9947	5–8	0.9948	< 5	0.9953		
A_6 lump	5–8	0.9944	1–5	0.9969	< 5	0.9963				
A_7 lump	1–5	0.9969	< 1	0.8845						
A_8 lump	< 1	0.9269								
RSS	5.18×10^{-3}	6.72×10^{-3}	5.36×10^{-3}	6.02×10^{-3}	7.33×10^{-3}					

Note: M_W is the molecular weight of the degraded chitosan. RSS is the residual sum of squares.

Table 3 Chromatographic quantitative analysis results for degradation products at 30 °C at different time.

t/min	Concentration/mg·mL^{-1}						c_A/mg·mL^{-1}
	A_1 lump	A_2 lump	A_3 lump	A_4 lump	A_5 lump	A_6 lump	
0	0.5909	0.4316	0.1111	0.0278	0.0457	0.0908	1.2979
5	0.4773	0.4960	0.1396	0.0347	0.0560	0.0904	1.2939
10	0.3969	0.5361	0.1677	0.0430	0.0701	0.1345	1.3483
15	0.3357	0.5437	0.1825	0.0473	0.0772	0.1105	1.2970
20	0.2690	0.5434	0.1991	0.0524	0.0858	0.1248	1.2745
25	0.2186	0.5434	0.2189	0.0589	0.0970	0.1456	1.2824
30	0.1627	0.5401	0.2498	0.0702	0.1186	0.1747	1.3160
35	0.1286	0.5231	0.2642	0.0765	0.1310	0.2079	1.3314
40	0.0972	0.4840	0.2666	0.0789	0.1369	0.2252	1.2889
45	0.0740	0.4498	0.2700	0.0823	0.1446	0.2419	1.2626
50	0.0627	0.4317	0.2786	0.0870	0.1554	0.2623	1.2777
60	0.0403	0.3863	0.2930	0.0970	0.1794	0.3202	1.3161
70	0.0224	0.3201	0.2817	0.0980	0.1865	0.3540	1.2628
80	0.0151	0.2793	0.2792	0.1018	0.1993	0.3944	1.2692
90	0.0085	0.2277	0.2663	0.1025	0.2081	0.4576	1.2707
100	0.0039	0.1830	0.2543	0.1045	0.2203	0.4961	1.2619
110	0.0026	0.1474	0.2344	0.1018	0.2233	0.5503	1.2598
120	0.0009	0.1211	0.2243	0.1026	0.2328	0.5958	1.2775

Note: c_A is the sum of the concentration of six lumps.

Table 4 Parameters estimation results and fitting error of lumping model.

k/min^{-1}	Temperature°C				Relative error/%	Temperature/°C			
	30	40	50	60		30	40	50	60
k_{11}	3.69×10^{-2}	4.09×10^{-2}	5.98×10^{-2}	1.63×10^{-1}	A_1 lump	−12.85	−18.14	–22.42	−30.56
k_{12}	6.54×10^{-3}	1.07×10^{-3}	1.39×10^{-6}	2.17×10^{-12}	A_2 lump	−4.67	−1.27	−12.31	−14.50
k_{13}	3.49×10^{-3}	5.86×10^{-8}	6.14×10^{-5}	5.61×10^{-12}	A_3 lump	−4.76	−0.07	−1.29	−10.90
k_{14}	2.68×10^{-3}	4.56×10^{-11}	3.99×10^{-6}	2.01×10^{-11}	A_4 lump	−13.08	−1.18	2.09	−6.23
k_{15}	2.66×10^{-3}	9.11×10^{-9}	8.05×10^{-6}	2.22×10^{-14}	A_5 lump	−7.39	−0.71	0.78	−14.82
k_{21}	9.64×10^{-3}	1.30×10^{-2}	2.37×10^{-2}	7.73×10^{-2}	A_6 lump	−4.64	−1.43	−0.29	−0.46
k_{22}	1.08×10^{-3}	2.85×10^{-3}	2.67×10^{-3}	4.37×10^{-7}					
k_{23}	3.56×10^{-3}	3.97×10^{-3}	3.13×10^{-3}	1.12×10^{-3}					
k_{24}	3.07×10^{-3}	9.45×10^{-8}	1.86×10^{-3}	1.11×10^{-2}					
k_{31}	4.83×10^{-4}	1.27×10^{-3}	1.28×10^{-2}	6.19×10^{-2}					
k_{32}	1.78×10^{-3}	2.11×10^{-3}	9.65×10^{-3}	3.78×10^{-2}					
k_{33}	9.47×10^{-3}	1.26×10^{-2}	8.87×10^{-3}	1.93×10^{-3}					
k_{41}	7.08×10^{-8}	1.69×10^{-3}	3.94×10^{-2}	1.59×10^{-1}					
k_{42}	1.01×10^{-9}	6.55×10^{-3}	1.35×10^{-8}	2.34×10^{-14}					
k_{51}	1.70×10^{-3}	3.38×10^{-3}	2.72×10^{-2}	1.02×10^{-1}					

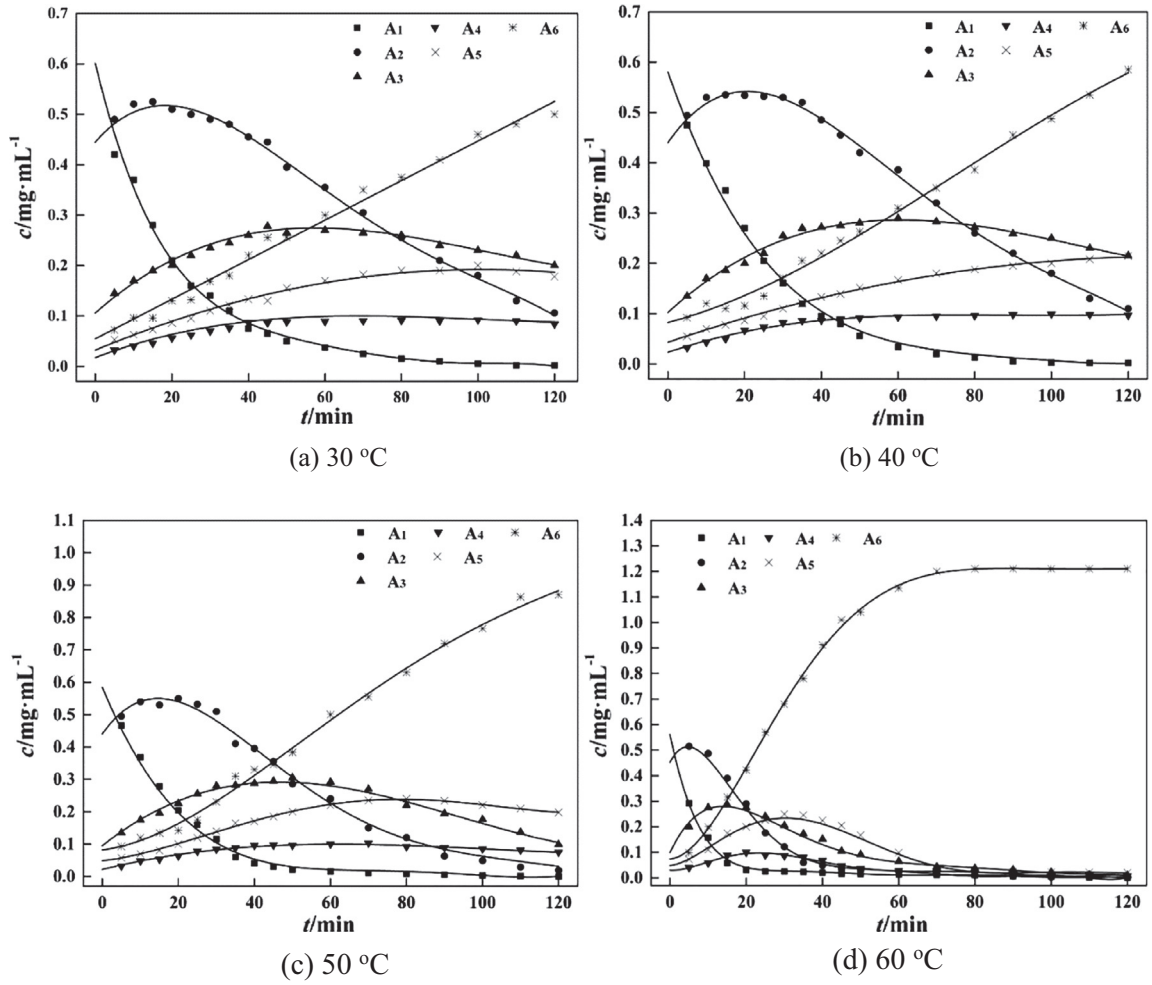

Fig. 5 Chitosan degradation curves at different temperatures. line-calculated value; dot-experimented value; t-degradation time; c-product concentration.

atures. The errors of fitting results at 30 °C, 40 °C and 50 °C were small, especially those at 40 °C. The results showed that the six-lumped kinetic model can well-describe the distribution of degradation products of chitosan by hydrodynamic cavitation.

It can be seen from Fig. 5**(a)–(d)** that the concentrations of lump A_1 with the largest molecular weight declined over time at different degradation temperatures. The degradation rates of lump A_1 increased with the increase of temperatures. In contrast, the concentrations of lump A_6 with the lowest molecular weight increased over time at different degradation temperatures, and the formation rate of lump A_6 was accelerated significantly with the increase of temperatures. At the early stages of the reactions, the formation rates of lumps A_2 and A_3 were higher than the degradation rates of A_2 and A_3, leading to the increase of their concentrations. With the proceeding of the degradation reactions, the concentrations of lumps A_2 and A_3 declined because the degradation rates surpassed the formation rates. The concentrations of lumps A_4 and A_5 showed an increasing trend at 30 and 40 °C, while they first increased and then decreased at 50 and 60 °C. The main reason could be that at low temperatures such as 30 and 40 °C, the degradation rates of all the lumps were relatively low. With the increase of temperature, the degradation reactions were accelerated. The degradation reactions reached a high level in a short time, and the degradation degree of chitosan was higher.

Fig. 5**(d)** shows that at 60 °C, the lumps A_1, A_2, A_3, A_4 and A_5 almost completely degraded after 70 min of reactions, and the mass concentration of lump A_6 tended to be constant. The results show that the reaction rates could be obviously improved by increasing the temperatures of reactions. A higher temperature facilitated the degradation process (Huang et al., 2013). The degradation temperature and degradation time were vital to the degradation of chitosan. Products with medium molecular weights were obtained at lower reaction temperatures or shorter reaction time, while products with low molecular weights were obtained at higher reaction temperatures or over longer reaction time. In summary, the composition and distribution of chitosan degradation products can be controlled by adjusting the reaction time and temperature.

3.4. Activation energy results of lumped reactions

The correlations between reaction rate constants ln$k$ and 1/T corresponding to the points on the diagonal of the six-

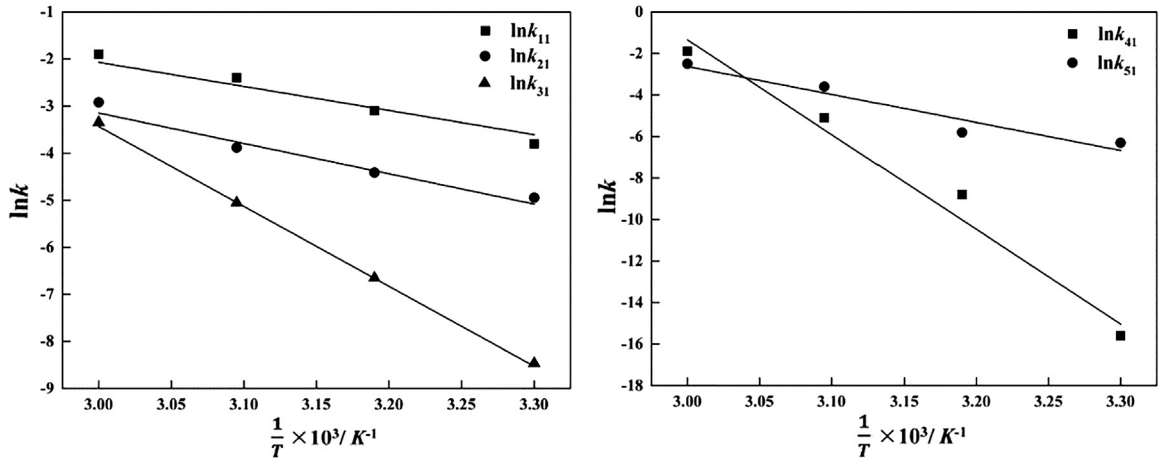

Fig. 6 Reaction rate constants with temperature. T-temperature; k-reaction rate constants.

lumped reaction network at 30 ~ 60 °C are illustrated in Fig. 6. The correlations were in good accordance with the Arrhenius equation, and the corresponding activation energy values were calculated to be 40 ~ 399 kJ·mol^{-1}. The corresponding equations are given as follow:

$$lnk_{11} = 12.413 - \frac{4.8279}{T} \quad (11)$$

$$lnk_{21} = 17.757 - \frac{6.8569}{T} \quad (12)$$

$$lnk_{31} = 48.082 - \frac{16.982}{T} \quad (13)$$

$$lnk_{41} = 144.13 - \frac{48.016}{T} \quad (14)$$

$$lnk_{51} = 41.038 - \frac{14.466}{T} \quad (15)$$

3.5. Prediction ability of the model

The prediction ability of the model and reliability of kinetic parameters obtained by fitting were assessed by comparing the fitting results with data derived in other experiments under different degradation reaction conditions. The degradation reactions were carried out at 35 and 45 °C, and the samples were withdrawn at 0, 8, 16, 24, 32, 42, 55, 65, 75, 85, 95, 105, 115, 120 min.

The values calculated and measured are depicted in Tables 5 and 6. Most of the average absolute deviations were < 9.3%, except the prediction deviation for the lump A_1. The large deviation for the lump A_1 may be due to that the degradation products contained chitosan with molecular weights beyond the detection range of the gel permeation chromatograph. Another reason may be that the range of molecular weights of chitosan in the lump A_1 was large, resulting in different kinetic properties of certain products. In addition, the large number of parameters could also increase the errors for the rate constant estimated. The average absolute deviations for lumps A_2, A_3 and A_6

Table 5 Comparison between calculated values of six lumps and experimental values at 35 °C.

t/min	A_1 lump/mg·mL^{-1}		A_2 lump/mg·mL^{-1}		A_3 lump/mg·mL^{-1}		A_4 lump/mg·mL^{-1}		A_5 lump/mg·mL^{-1}		A_6 lump/mg·mL^{-1}	
	Exp.	Cal.	Exp.	Cal.	Exp.	Cal.	Exp.	Cal.	Exp.	Cal.	Exp.	Cal.
8	0.3721	0.3879	0.4505	0.5086	0.1345	0.1472	0.0342	0.0358	0.0558	0.0598	0.0863	0.0986
16	0.3044	0.2568	0.5673	0.5341	0.2009	0.1914	0.0532	0.0475	0.0882	0.0793	0.1367	0.1288
24	0.1965	0.1700	0.5399	0.5178	0.2300	0.2286	0.0634	0.0595	0.1059	0.1001	0.1718	0.1620
32	0.1266	0.1125	0.5150	0.4792	0.2558	0.2560	0.0735	0.0706	0.1258	0.1214	0.2147	0.1983
42	0.0729	0.0672	0.4626	0.4179	0.2838	0.2759	0.0872	0.0820	0.1543	0.1471	0.2538	0.2479
55	0.0331	0.0344	0.3634	0.3356	0.2852	0.2812	0.0949	0.0917	0.1752	0.1762	0.3082	0.3188
65	0.0151	0.0205	0.2893	0.2779	0.2898	0.2734	0.1051	0.0953	0.2049	0.1935	0.4081	0.3773
75	0.0077	0.0123	0.2329	0.2274	0.2722	0.2586	0.1042	0.0957	0.2097	0.2059	0.4430	0.4381
85	0.0037	0.0073	0.1933	0.1846	0.2628	0.2394	0.1062	0.0936	0.2217	0.2130	0.5078	0.5000
95	0.0017	0.0044	0.1513	0.1490	0.2483	0.2178	0.1081	0.0895	0.2370	0.2153	0.5966	0.5620
105	0.0005	0.0026	0.0989	0.1197	0.1997	0.1955	0.0937	0.0840	0.2154	0.2132	0.5722	0.6230
115	0.0002	0.0016	0.0714	0.0959	0.1799	0.1734	0.0929	0.0776	0.2289	0.2075	0.7121	0.6821
120	0.0006	0.0012	0.0543	0.0858	0.1576	0.1627	0.0864	0.0742	0.2215	0.2035	0.7523	0.7106
MAD/%	−24.35%		−2.95%		2.78%		9.25%		4.31%		1.88%	

Note:MAD is the mean absolute deviation. Exp. is the observed value by experiment. Cal. is the calculated value by lumped model.

Table 6 Comparison between calculated values of six lumps and experimental values at 45 °C.

t/min	A_1 lump/mg·mL^{-1}		A_2 lump/mg·mL^{-1}		A_3 lump/mg·mL^{-1}		A_4 lump/mg·mL^{-1}		A_5 lump/mg·mL^{-1}		A_6 lump/mg·mL^{-1}	
	Exp.	Cal.	Exp.	Cal.	Exp.	Cal.	Exp.	Cal.	Exp.	Cal.	Exp.	Cal.
8	0.3777	0.3649	0.4893	0.4944	0.1501	0.1415	0.0381	0.0348	0.0622	0.0578	0.1001	0.0936
16	0.2692	0.2356	0.5416	0.5183	0.1990	0.1825	0.0528	0.0455	0.0874	0.0776	0.1463	0.1278
24	0.1668	0.1521	0.4951	0.4973	0.2139	0.2171	0.0591	0.0559	0.0990	0.0985	0.1583	0.1660
32	0.0929	0.0982	0.4744	0.4545	0.2655	0.2428	0.0792	0.0654	0.1384	0.1191	0.2389	0.2070
42	0.0457	0.0569	0.3786	0.3893	0.2551	0.2619	0.0804	0.0753	0.1438	0.1431	0.2443	0.2605
55	0.0240	0.0279	0.3295	0.3051	0.2842	0.2683	0.0977	0.0846	0.1848	0.1695	0.3691	0.3315
65	0.0135	0.0162	0.2737	0.2478	0.2787	0.2624	0.1012	0.0893	0.1969	0.1856	0.3827	0.3858
75	0.0058	0.0094	0.2016	0.1989	0.2504	0.2500	0.0968	0.0921	0.1975	0.1978	0.4256	0.4389
85	0.0023	0.0054	0.1527	0.1583	0.2328	0.2334	0.0983	0.0933	0.2113	0.2063	0.4953	0.4903
95	0.0016	0.0031	0.1286	0.1253	0.2203	0.2144	0.0974	0.0932	0.2161	0.2114	0.5462	0.5396
105	0.0006	0.0018	0.0976	0.0988	0.2029	0.1944	0.0965	0.092	0.2248	0.2135	0.6209	0.5864
115	0.0003	0.0010	0.0711	0.0776	0.1706	0.1744	0.0860	0.090	0.2087	0.2131	0.6363	0.6308
120	0.0003	0.0008	0.0620	0.0688	0.1585	0.1647	0.0819	0.0888	0.2020	0.2120	0.6193	0.6520
MAD/%	−26.75%		0.29%		2.40%		6.85%		3.97%		2.67%	

Note:MAD is the mean absolute deviation. Exp. is the observed value by experiment. Cal. is the calculated value by lumped model.

were < 3%, and those for A_4 and A_5 were slightly larger. The reason is that the degradation rates of chitosan were low at 35 °C and 45 °C, and the lumps A_4 and A_5 did not completely degrade. The analysis results indicated that multi-parameter lumped kinetic models can quantitatively predict the degradation process of chitosan and concentration distribution of lumped components in the reaction networks.

4. Conclusion

In this work, the lumped kinetics of chitosan degradation by hydrodynamic cavitation was investigated. The six-lumped model showed a better prediction ability with most of the average absolute deviations < 9.3%, and the parameters estimated were uncomplicated. The six-lumped reaction kinetic parameters showed that the degradation reactions of chitosan mainly occurred on the diagonal of the reaction network. The maximum value of the kinetic parameters on the diagonal (1.63×10^{-1}) was much larger than that of non-diagonal kinetic parameters (3.78×10^{-2}). Namely, lumps with close molecular weights were mainly generated in the degradation reactions. The multi-parameter six-lumped kinetic model quantitatively described the complex degradation process of chitosan by hydrodynamic cavitation, effectively predicted the concentration distribution of each lump, and resolved the concerns resulting from the diverse distributions of degradation products. This work is beneficial for the research on the kinetics of complex degradation reactions of chitosan and other polysaccharides.

Declaration of Competing Interest

The authors declare that they have no known competing financial interests or personal relationships that could have appeared to influence the work reported in this paper.

Acknowledgements

This work was supported by the National Natural Science Foundation of China (NO.31660472).

References

Beers, K.J., 2006. Numerical Methods with Chemical Engineering Applications in MATLAB. Cambridge University Press, England.

Capocelli, M., Prisciandaro, M., Lancia, A., Musmarra, D., 2013. Modeling of cavitation as an advanced wastewater treatment. Desalin. Water Treat. 51, 1609–1614. https://doi.org/10.1080/19443994.2012.705094.

Chuah, L.F., Klemeš, J.J., Yusup, S., Bokhari, A., Akbar, M.M., 2017. A review of cleaner intensification technologies in biodiesel production. J. Clean. Prod. 146, 181–193. https://doi.org/10.1016/j.jclepro.2016.05.017.

Chuah, L.F., Yusup, S., Abd Aziz, A.R., Bokhari, A., Abdullah, M.Z., 2016. Cleaner production of methyl ester using waste cooking oil derived from palm olein using a hydrodynamic cavitation reactor. J. Clean. Prod. 112 (5), 4505–4514. https://doi.org/10.1016/j.jclepro.2015.06.112.

Chuah, L.F., Yusup, S., Abd Aziz, A.R., Bokhari, A., Klemeš, J.J., Abdullah, M.Z., 2015. Intensification of biodiesel synthesis from waste cooking oil (palm olein) in a hydrodynamic cavitation reactor: effect of operating parameters on methyl ester conversion. Chem. Eng. Process. 95, 235–240. https://doi.org/10.1016/j.cep.2015.06.018.

Czech, B., Zygmunt, P., Kadirova, Z.C., Yubuta, K., Hojamberdiev, M., 2020. Effective photocatalytic removal of selected pharmaceuticals and personal care products by elsmoreite/tungsten oxide@ZnS photocatalyst. J. Environ. Manage. 270,. https://doi.org/10.1016/j.jenvman.2020.110870 110870.

Huang, H., 2004. Practical computer simulation of chemical processes : MATLAB's applicat. Chemical Idustry, China.

Huang, Y., Wang, P., Yuan, Y., Ren, X., Yang, F., 2015. Synergistic degradation of chitosan by impinging stream and jet cavitation. Ultrason. Sonochem. 27, 592–601. https://doi.org/10.1016/j.ultsonch.2015.04.019.

Huang, Y., Wu, Y., Huang, W., Yang, F., Ren, X.E., 2013. Degradation of chitosan by hydrodynamic cavitation. Polym. Degrad. Stab. 98, 37–43. https://doi.org/10.1016/j.polymdegradstab.2012.11.001.

Iovino, P., Chianese, S., Canzano, S., Prisciandaro, M., Musmarra, D., 2016. Degradation of Ibuprofen in Aqueous Solution with UV Light: the Effect of Reactor Volume and pH. Water. Air. Soil Pollut. 227, 194. https://doi.org/10.1007/s11270-016-2890-3.

John, Y.M., Mustafa, M.A., Patel, R., Mujtaba, I.M., 2019. Parameter estimation of a six-lump kinetic model of an industrial fluid catalytic cracking unit. Fuel 235, 1436–1454. https://doi.org/10.1016/j.fuel.2018.08.033.

Kim, S.K., Rajapakse, N., 2005. Enzymatic production and biological activities of chitosan oligosaccharides (COS): A review. Carbohydr. Polym. 62, 357–368. https://doi.org/10.1016/j.carbpol.2005.08.012.

Kumar, M.N.V.R., 2000. A review of chitin and chitosan applications, Reactive & Functional Polymers. Reactive Functical Polym. 46, 1–27. https://doi.org/10.1016/S1381-5148(00)00038-9.

Kyoon No, H., Park, N.Y., Lee, S.H., Meyers, S.P., 2002. Antibacterial activity of chitosans and chitosan oligomers with different molecular weights. Int. J. Food Microbiol. 74 (1–2), 65–72. https://doi.org/10.1016/S0168-1605(01)00717-6.

Lee, H.C., Chang, T., 1996. Polymer molecular weight characterization by temperature gradient high performance liquid chromatography. Polymer 37 (25), 5747–5749. https://doi.org/10.1016/S0032-3861(96)00510-1.

Lee, M.Y., Var, F., Shin-ya, Y., Kajiuchi, T., Yang, J.W., 1999. Optimum conditions for the precipitation of chitosan oligomers with DP 5–7 in concentrated hydrochloric acid at low temperature. Process Biochem. 34, 493–500. https://doi.org/10.1016/S0032-9592(98)00116-2.

Liu, H., Zhu, X., Zhang, X., Wang, Z., Sun, B., 2019. Photodegradation of Oxytetracycline in the Presence of Dissolved Organic Matter and Chloride Ions: Importance of Reactive Chlorine Species. Water. Air. Soil Pollut. 230, 235. https://doi.org/10.1007/s11270-019-4293-8.

Mei, Y., Dai, X., Yang, W., Xu, X., Liang, Y., 2015. Antifungal activity of chitooligosaccharides against the dermatophyte Trichophyton rubrum. Int. J. Biol. Macromol. 77, 330–335. https://doi.org/10.1016/j.ijbiomac.2015.03.042.

Moore, J., 1964. Gel permeation chromatography. I. A new method for molecular weight distribution of high polymers. J. Polym. Sci. Part A Gen. Pap. 2, 835–843. https://doi.org/10.1002/pol.1964.100020220.

Mourya, V.K., Inamdar, N.N., Choudhari, Y.M., 2011. Chitooligosaccharides: Synthesis, characterization and applications. Polym. Sci. - Ser. A 53, 583–612. https://doi.org/10.1134/S0965545X11070066.

Muley, A.B., Shingote, P.R., Patil, A.P., Dalvi, S.G., Suprasanna, P., 2019. Gamma radiation degradation of chitosan for application in growth promotion and induction of stress tolerance in potato (Solanum tuberosum L.). Carbohydr. Polym. 210, 289–301. https://doi.org/10.1016/j.carbpol.2019.01.056.

Negm, N.A., Hefni, H.H.H., Abd-Elaal, A.A.A., Badr, E.A., Abou Kana, M.T.H., 2020. Advancement on modification of chitosan biopolymer and its potential applications. Int. J. Biol. Macromol. 152, 681–702. https://doi.org/10.1016/j.ijbiomac.2020.02.196.

Ren, D., Yi, H., Xie, W., Ma, X., 2006. Study on homogeneity of enzymatic degradation of chitosan as biomaterials by gel permeation chromatography. Chinese J. Chromatogr. 24, 407. https://doi.org/10.1016/S1872-2059(06)60017-5.

Rinaudo, M., 2006. Chitin and chitosan: Properties and applications. Prog. Polym. Sci. 31 (7), 603–632. https://doi.org/10.1016/j.progpolymsci.2006.06.001.

Shi, D., He, Z., Qi, W., 2005. Lumping kinetic study on the process of tryptic hydrolysis of bovine serum albumin. Process Biochem. 40, 1943–1949. https://doi.org/10.1016/j.procbio.2004.07.009.

Song, X., Chen, Y., Zhao, G., Sun, H., Che, H., Leng, X., 2020. Effect of molecular weight of chitosan and its oligosaccharides on antitumor activities of chitosan-selenium nanoparticles. Carbohydr. Polym. 231. https://doi.org/10.1016/j.carbpol.2019.115689.

Tian, F., Liu, Y., Hu, K., Zhao, B., 2004. Study of the depolymerization behavior of chitosan by hydrogen peroxide. Carbohydr. Polym. 57, 31–37. https://doi.org/10.1016/j.carbpol.2004.03.016.

Wu, Y., Huang, Y., Zhou, Y., Ren, X., Yang, F., 2014. Degradation of chitosan by swirling cavitation. Innov. Food Sci. Emerg. Technol. 23, 188–193. https://doi.org/10.1016/j.ifset.2014.02.001.

Xia, W., Liu, P., Zhang, J., Chen, J., 2011. Biological activities of chitosan and chitooligosaccharides. Food Hydrocoll. 25, 170–179. https://doi.org/10.1016/j.foodhyd.2010.03.003.

Yan, J., Ai, S., Yang, F., Zhang, K., Huang, Y., 2020a. Study on mechanism of chitosan degradation with hydrodynamic cavitation. Ultrason. Sonochem. 64,. https://doi.org/10.1016/j.ultsonch.2020.105046 105046.

Yan, J., Xu, J., Ai, S., Zhang, K., Yang, F., Huang, Y., 2020b. Degradation of chitosan with self-resonating cavitation. Arab. J. Chem. 13 (6), 5776–5787. https://doi.org/10.1016/j.arabjc.2020.04.015.

Zaharoff, D.A., Rogers, C.J., Hance, K.W., Schlom, J., Greiner, J.W., 2007. Chitosan solution enhances both humoral and cell-mediated immune responses to subcutaneous vaccination. Vaccine 25, 2085–2094. https://doi.org/10.1016/j.vaccine.2006.11.034.

Zhang, D., Ren, Z., Wang, D., Lu, K., 2017. Upgrading of crude oil in supercritical water: A five-lumped kinetic model. J. Anal. Appl. Pyrol. 123, 56–64. https://doi.org/10.1016/j.jaap.2016.12.025.

Zhao, Z., Liao, D., Sun, J., Huang, K., Sun, G., Jin, W., Xie, M., Zhihong, W.U., Tong, Z., 2011. Lumping kinetic model of enzymatic hydrolysis of protein of silkworm pupae-alcalase system. Ciesc J. 62 (09), 2588–2594. https://doi.org/10.1016/S1005-0302(11)60031-5.

Zou, P., Yang, X., Wang, J., Li, Y., Yu, H., Zhang, Y., Liu, G., 2016. Advances in characterisation and biological activities of chitosan and chitosan oligosaccharides. Food Chem 190, 1174–1181. https://doi.org/10.1016/j.foodchem.2015.06.076.